Available online at www.sciencedirect.com
ScienceDirect
Journal of Power Sources 159 (2006) 1071–1077
JOURNAL OF POWER SOURCES
www.elsevier.com/locate/jpowsour

Transient behavior of CO poisoning of the anode catalyst layer of a PEM fuel cell

H.S. Chu [a], C.P. Wang [a], W.C. Liao [a], W.M. Yan [b,*]

[a] *Department of Mechanical Engineering, National Chiao Tung University, Hsinchu, Taiwan 300, ROC*
[b] *Department of Mechatronic Engineering, Huafan University, Shih Ting, Taipei, Taiwan 223, ROC*

Received 4 October 2005; received in revised form 20 December 2005; accepted 20 December 2005
Available online 3 February 2006

Abstract

A one-dimensional transient mathematical model is applied to simulate the carbon monoxide poisoning effect on the performance of a PEM fuel cell. Based on the CO kinetic model developed by Springer et al. [T.E. Springer, T. Rockward, T.A. Zawodzinski, S. Gottesfeld, J. Electrochem. Soc. 148 (2001) A11–A23], the transient behaviors of the CO poisoning process across the anode catalyst layer is investigated. The results show that the hydrogen coverage, θ_H, decreases with the time due to CO adsorption on the catalyst sites. A higher CO concentration results in fewer available catalyst sites for hydrogen electro-oxidation and a significant decrease in the response time to reach steady state, t_{ss}. Increasing the anode overpotential and the gas porosity would result in an increase in the current density, especially at low levels of CO concentration.

Keywords: PEM fuel cell; Unsteady state; CO poisoning; Anode catalyst layer

1. Introduction

Fuel cell performance and durability are strongly influenced by impurities in the hydrogen fuel gas. Reforming of methanol or gasoline fuels is the most widely used method to generate the hydrogen fuel which contains 45% hydrogen, 10 ppm CO, 15% CO_2, and 1% CH_4 [1]. Nevertheless, 5–10 ppm CO would reduce the hydrogen electro-oxidation effectively by occupying the Pt reacting surface sites which results in a decrease in the cell performance [2]. To keep maintain long and stable operation, how to reduce the CO concentration effectively from the reformer and enhance the CO tolerance of the fuel cell will become a significant topic.

Many researchers have focused their interest on the effects of the impurities ions from both hydrogen fuel and air on the cell performance. Okada et al. [3–7] have examined the water transport in the membrane of the fuel cell with the effects of the impurity ions. Water content, electricity, transference coefficient, and water permeability decrease with an increase in the impurity ions. Halseid et al. [8] indicated that the cell performance was also influenced the ammonia from the reformer. A higher concentration of ammonia ions caused a lower membrane conductivity. To reduce the decay of the cell performance, Uribe et al. [9] used a Pt–Ru alloy to slow down the performance decay. The CO tolerance of a carbon-supported platinum–ruthenium catalyst at elevated temperatures and atmospheric pressure in a PEM fuel cell was investigated by Si et al. [10]. They indicated that the CO became dissociated from the platinum reaction sites at high operation temperatures which possess a high CO tolerance and can provide more catalyst sites for hydrogen.

Zhang et al. [11] found that the CO poisoning process can be accelerated at a high mass flow rate. However, increasing cathode pressure can raise the oxygen diffusion from cathode to anode side and assist in CO oxidation on the anode catalyst. In the other studies [12,13], the promotion of CO tolerance can be achieved by adopting different cell structure designs. Yu et al. [12] used the Pt–Ru alloy as a filter to reduce the CO poisoning. In their study, the Pt–Ru alloy was placed between the gas diffusion layer and the catalyst layer. In a similar way, Santiago et al. [13] used Ru metal to fabricate the gas diffusion layer. Before the CO entered into the catalyst layer, the high oxidation ability of Ru oxidized the CO to CO_2. It is concluded from Refs. [12,13] that the CO poisoning effect can be reduced by a simple structure. But, the fabrication cost was increased. To avoid the

* Corresponding author. Tel.: +886 2 26632102; fax: +886 2 26632143.
E-mail address: wmyan@huafan.hfu.edu.tw (W.M. Yan).

0378-7753/$ – see front matter © 2006 Elsevier B.V. All rights reserved.
doi:10.1016/j.jpowsour.2005.12.045

Nomenclature

a	contact area of Pt catalyst ($cm^2\ cm^{-3}$)
b_{fCO}	ratio of forward to backward of CO adsorption (atm)
b_{fH}	ratio of forward to backward of hydrogen adsorption (atm)
C	concentration of reactant gas ($mol\ cm^{-3}$)
D	diffusion coefficient ($cm^2\ s^{-1}$)
ΔE_H	activation energy change for hydrogen dissociative adsorption near CO occupied sites ($J\ mol^{-1}$)
ΔG_f	variation of free energy of CO adsorption between zero and full coverage ($J\ mol^{-1}$)
i	current density ($A\ cm^{-2}$)
k_{eCO}	CO electro-oxidation rate constant ($A\ cm^{-2}$)
k_{eH}	hydrogen electro-oxidation rate constant ($A\ cm^{-2}$)
k_{fCO}	CO adsorption rate constant ($A\ cm^{-2}\ atm^{-1}$)
k_{fH}	hydrogen adsorption rate constant ($A\ cm^{-2}\ atm^{-1}$)
n	number of electrons
P	total pressure (atm)
R	universal gas constant ($J\ mol^{-1}\ K^{-1}$)
s	stoichiometric coefficient
t	time (s)
T	temperature (K)
X	molar fraction
z	distance (μm)

Greek letters

ε	porosity
η	overpotential (V)
θ_{CO}	coverage ratio of CO on Pt catalyst site
θ_H	coverage ratio of hydrogen on Pt catalyst site
ξ	molar area density of Pt catalyst sites ($C\ cm^{-2}$)
ϕ	potential (V)

Subscripts

CO	carbon monoxide
H_2	hydrogen gas
ss	steady state

Superscripts

in	inlet at catalyst layer ($z = 0$)
0	initial state

use of a precious metal, some researchers adopted some methods to restore the cell performance during the operation process, including oxidant-bleeding [14–16], self-oxidation [2,17], and current-pulsing [17,18].

In theoretical studies, Springer et al. [19] derived a mathematical model to describe CO adsorption, desorption and charge fluxes on the Pt catalyst site. The adsorption phenomena of hydrogen and carbon monoxide on the Pt catalyst are the main mechanisms which cause the deterioration in the cell performance. In addition, the relationship between the rate constant and the coverage ratio was proposed by Springer et al. Chan et al. [20] combined the theoretical models developed by Springer et al. [19] and Bernardi et al. [21,22] to examine the CO kinetics. The steady-state fuel gas and coverage profiles were presented for different CO concentrations. Bhatia and Wang [23] treated the anode catalyst layer as a boundary condition to analyze the transient CO poisoning behaviors at different CO levels. A simple relationship between rate constants and coverage was used. Baschuk and Li [24–27] studied the CO poisoning and O_2 bleeding in a PEM fuel cell to reduce the poisoning effect of CO. Although the transient variations of the fuel cell performance under different CO concentrations were observed, the actual transient coverage profiles and the reactant gas distributions across the anode catalyst layer were not presented.

In the present study, a transient one-dimensional mathematical model of the CO poisoning behavior in a PEM fuel cell was studied. In order to improve the cell performance, several physical parameters are considered to promote CO tolerance and analyze the influence on the response time, t_{ss}.

1.1. Theoretical model

Consider an anode catalyst layer of thickness L_c, as schematically shown in Fig. 1. Transient analysis of CO poisoning behavior across the anode catalyst layer is investigated. The theoretical model of CO kinetics proposed by Springer et al. [19] was adopted in this work. For hydrogen, CO, and Pt interfacial kinetics, four expressions are described as follows:

$$H_2 + 2Pt \leftrightarrow 2(H - Pt) \quad (1)$$

$$CO + Pt \leftrightarrow (CO - Pt) \quad (2)$$

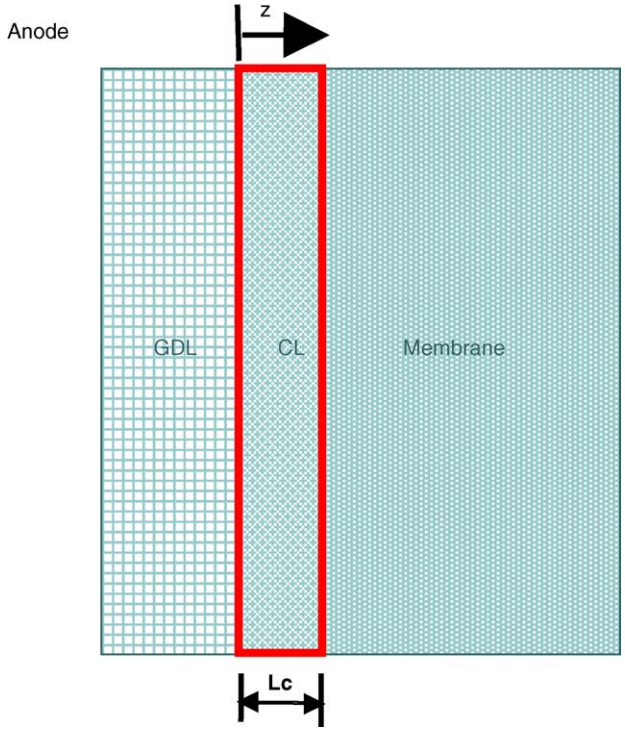

Fig. 1. A schematic model for the anode domain of the PEM fuel cell.

$$(CO - Pt) + H_2O \rightarrow Pt + CO_2 + 2H^+ + 2e^- \quad (3)$$

$$H - Pt \rightarrow Pt + H^+ + e^- \quad (4)$$

Hydrogen dissociative chemisorption and the CO adsorption on the Pt catalyst sites are described by Eqs. (1) and (2), respectively. In the above equations, Eqs. (3) and (4) represent the CO and hydrogen electro-oxidation, respectively. Under the time-dependent conditions, Eqs. (5) and (6) describe the first order transient process of adsorption, desorption and charge fluxes:

$$\xi\frac{d\theta_H}{dt} = k_{fH} + X_{H_2}P(1-\theta_H-\theta_{CO}) - b_{fH}k_{fH}\theta_H - 2k_{eH}\theta_H \sin\left(\frac{n_{H_2}F\eta}{2RT}\right) \quad (5)$$

$$\xi\frac{d\theta_{CO}}{dt} = k_{fCO} + X_{CO}P(1-\theta_H-\theta_{CO}) - b_{fCO}k_{fCO}\theta_{CO} - 2k_{eCO}\theta_{CO} \sin\left(\frac{n_{CO}F\eta}{2RT}\right) \quad (6)$$

where θ_H and θ_{CO} denote the fraction of catalyst site coverage by hydrogen and CO, respectively. The forward rate constant of hydrogen and CO adsorption-to-desorption rate ratios are expressed as k_{FH} and b_{fc}, which are functions of CO coverage ratio and expressed as follows:

$$k_{fH} = k_{fH_0}\exp\left[-\frac{\delta(\Delta G_{CO})}{RT}\left(1-\exp\left(\frac{\lambda\theta_{CO}}{\theta_{CO}-1}\right)\right)\right] \quad (7)$$

$$b_{fCO} = b_{fCO_0}\exp\left[\frac{\delta(\Delta G_{CO})}{RT}\theta_{CO}\right] \quad (8)$$

Unsteady transport equations for H_2 and CO across the anode catalyst layer can be written as

$$\varepsilon_c\frac{\partial C_{H_2}}{\partial t} = \varepsilon_c D_{H_2}\frac{\partial^2 C_{H_2}}{\partial z^2} - \frac{di_{H_2}}{dz}\left(\frac{s_{H_2}}{n_{H_2}F}\right) \quad (9)$$

$$\varepsilon_c\frac{\partial C_{CO}}{\partial t} = \varepsilon_c D_{CO}\frac{\partial^2 C_{CO}}{\partial z^2} - \frac{di_{CO}}{dz}\left(\frac{s_{CO}}{n_{CO}F}\right) \quad (10)$$

where ε_c stands for the gas porosity, D_{H_2} and D_{CO} denote the diffusion coefficient of hydrogen and CO, respectively. s is the stoichiometric coefficient, n the number of electrons, F the Faraday constant, and $\frac{di}{dz}$ is the electro-chemical reactions which are described by Eqs. (11) and (12). Subscripts H_2 and CO represent the hydrogen and carbon monoxide, respectively. The operating current density is then:

$$\frac{di}{dz} = \frac{di_{H_2}}{dz} + \frac{di_{CO}}{dz} = 2ak_{eH}\theta_H \sin\left(\frac{n_{H_2}F\eta}{2RT}\right) + 4ak_{eCO}\theta_{CO}\sinh\left(\frac{n_{CO}F\eta}{2RT}\right) \quad (11)$$

To investigate the transient behaviors of the reactant gases distributions and coverage ratio distributions across the anode catalyst layer, the initial conditions are all set from zero which expressed as follows:

$$C_{H_2}(z,0) = C^0_{H_2}(z,0) \quad (12)$$

$$C_{CO}(z,0) = C^0_{CO}(z,0) \quad (13)$$

$$\theta_H(z,0) = \theta^0_H(z,0) \quad (14)$$

$$\theta_{CO}(z,0) = \theta^0_{CO}(z,0) \quad (15)$$

At the boundary $z=0$, the hydrogen and CO are given a fixed amount of concentration. At the interface between the anode catalyst layer and the membrane ($z=L_c$), the flux of reactant gases equal to zero. The corresponding boundary conditions are illustrated as follows:

$$C_{H_2} = C^{in}_{H_2}, \quad z=0 \quad (16)$$

$$C_{CO} = C^{in}_{CO}, \quad z=0 \quad (17)$$

$$D_{H_2}\frac{\partial C_{H_2}}{\partial z} = 0 \quad (18)$$

$$D_{CO}\frac{\partial C_{CO}}{\partial z} = 0 \quad (19)$$

Because no electro-oxidation occurs at the interface between the anode gas diffusion layer and the anode catalyst layer, the current density is set to be zero.

$$i = 0 \quad (20)$$

2. Results and discussion

To examine the transient behavior of the poisoning process, various CO concentrations are employed to simulate a wide range of hydrogen fuel from the reformer. Several physical parameters are considered to analyze the reactant gas distribution, coverage, current density, and the time response needed to reach the steady state condition after start-up operation. Table 1 presents the parameters used in this work.

Transient evolutions of the hydrogen and CO distributions across the anode catalyst layer with 100 ppm CO are shown in Fig. 2. Because of the fast kinetics of hydrogen, the current density was provided by the hydrogen electro-oxidation resulting in much lower concentration profiles. In contrast, the concentration distribution of CO was only depleted slightly across the anode catalyst layer. As a result, both the hydrogen and the CO concentrations take 541 s to reach the steady-state condition after start-up.

The transient distributions of the hydrogen coverage across the anode catalyst layer for 100 ppm CO are indicated in Fig. 3.

Table 1
The parameters used in the present model

T (K)	353
P (atm)	3
α	0.5
D_{H_2} ($cm^2\,s^{-1}$)	2.59×10^{-6}
k_{fH_0} ($A\,cm^{-2}\,atm$)	100
b_{Fh}	0.5
k_{Eh} ($A\,cm^{-2}$)	4
k_{ECO} ($A\,cm^{-2}\,atm$)	10
b_{fCO} (atm)	1.51×10^{-9}
k_{eCO} ($A\,cm^{-2}$)	1×10^{-8}

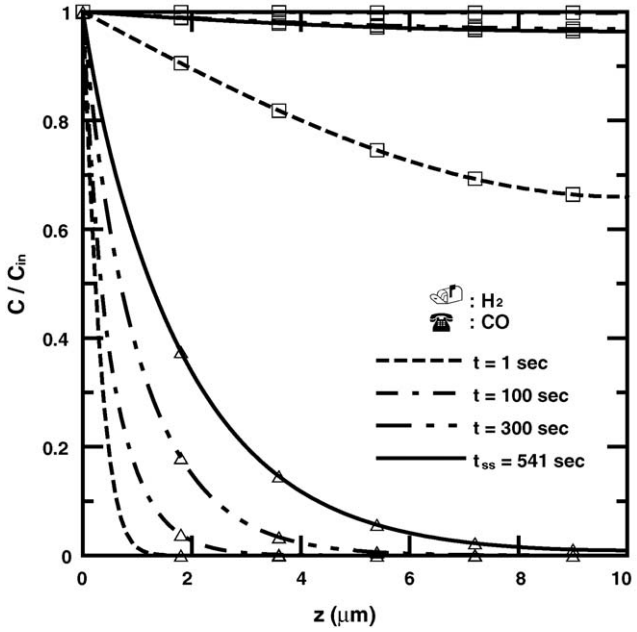

Fig. 2. Hydrogen (△) and carbon monoxide (□) distributions at various time steps across the anode catalyst layer for 100 ppm CO, $\varepsilon_c = 0.4$, $\eta_a = 0.01$, and $L_c = 10\,\mu m$.

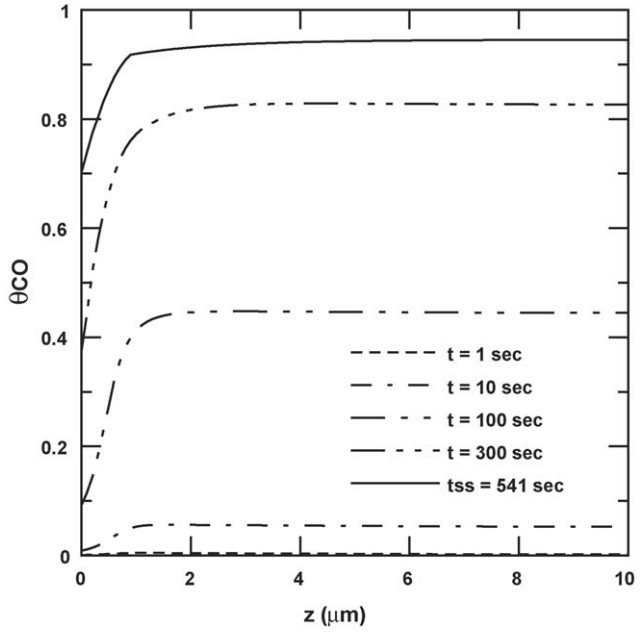

Fig. 4. Distributions of θ_{CO} at various time steps across the anode catalyst layer for 100 ppm CO, $\varepsilon_c = 0.4$, $\eta_a = 0.01$, and $L_c = 10\,\mu m$.

It is clearly seen that the hydrogen coverage, θ_H, decreases with time due to the CO adsorption on the catalyst sites. Owing to the high affinity between CO and the Pt catalyst, a large anode overpotential is needed to oxidize CO. As shown in Fig. 4, the catalyst sites are adsorbed onto by the CO with reaction time. This causes the hydrogen to diffuse deeply into the catalyst layer, which in turn, seeks more catalyst sites. Without extremely high overpotentials to make the CO oxidation, the accumulation of CO on the catalyst sites are sustained and therefore reduce hydrogen oxidation.

Fig. 5 shows the unsteady variations of the hydrogen oxidation current density across the anode catalyst layer. It is observed in Fig. 5 that the hydrogen oxidation increases sharply after the start-up operation (within the first 2 μm). Comparison of the corresponding hydrogen concentration distributions in Fig. 2 indicates that the fast kinetics of hydrogen results in a significant increase in the hydrogen oxidation current. In Fig. 6, the

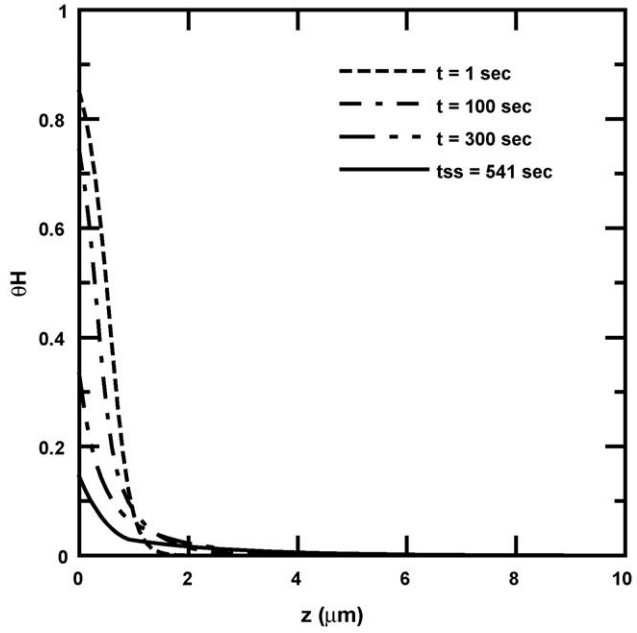

Fig. 3. Distributions of θ_H at various time steps across the anode catalyst layer for 100 ppm CO, $\varepsilon_c = 0.4$, $\eta_a = 0.01$, and $L_c = 10\,\mu m$.

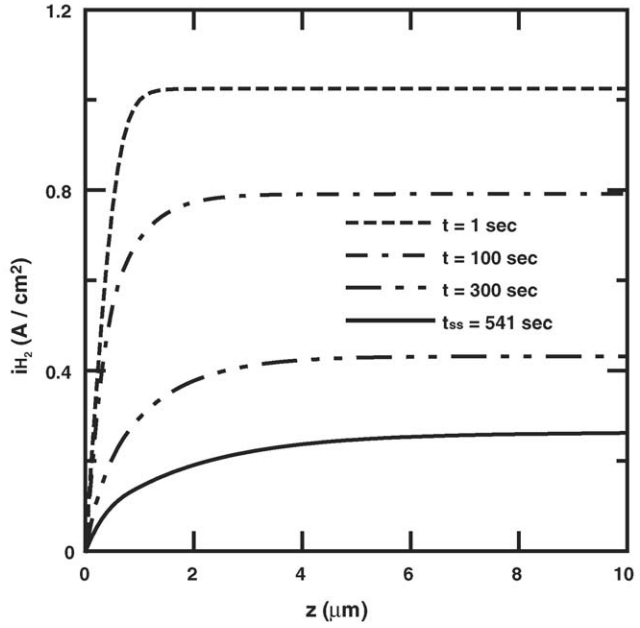

Fig. 5. Distributions of hydrogen oxidation current at various time steps across the anode catalyst layer for 100 ppm CO, $\varepsilon_c = 0.4$, $\eta_a = 0.01$, and $L_c = 10\,\mu m$.

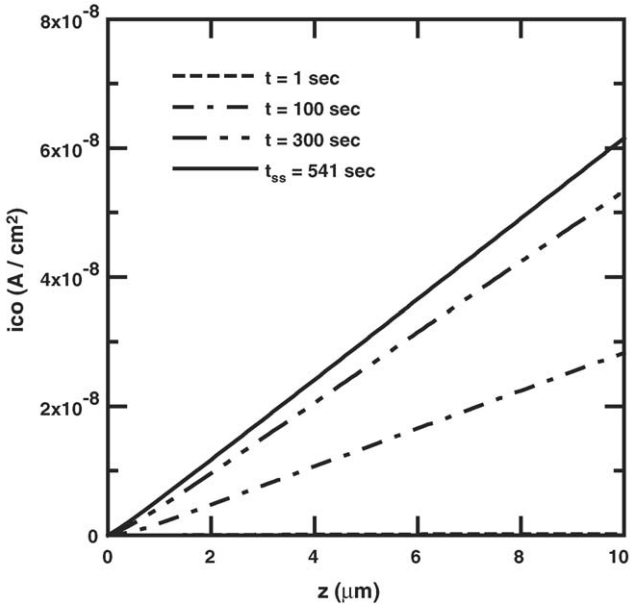

Fig. 6. Distributions of CO oxidation current at various time steps across the anode catalyst layer for 100 ppm CO, $\varepsilon_c = 0.4$, $\eta_a = 0.01$, and $L_c = 10\,\mu m$.

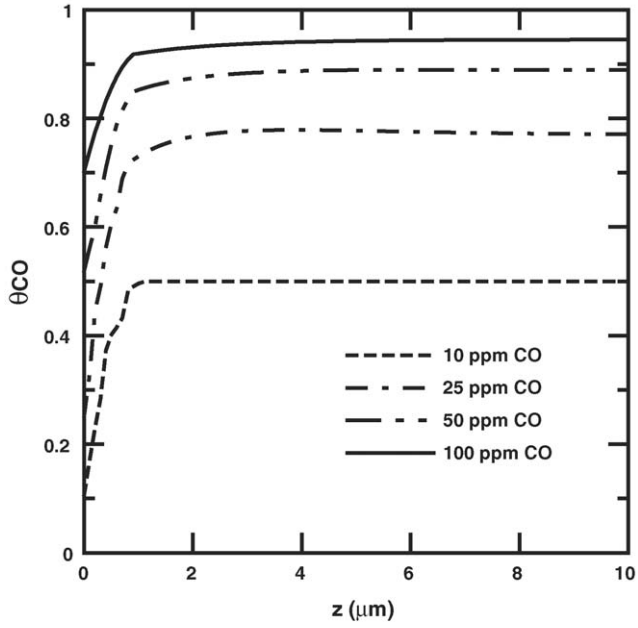

Fig. 8. Distributions of θ_{CO} at steady state across the anode catalyst layer for different CO concentrations with $\varepsilon_c = 0.4$, $\eta_a = 0.01$, and $L_c = 10\,\mu m$.

CO oxidation current is of the order of $10^{-8}\,A\,cm^{-2}$ which is much smaller than the hydrogen oxidation current. This implies that the CO oxidation current can be neglected.

Under various levels of the CO concentration from the reformer, the cell performance decreases with an increase in the CO concentration. Fig. 7 shows the steady-state hydrogen coverage under various CO concentrations in the range between 10 and 100 ppm. It is seen that the fuel with a high CO level would reduce the hydrogen coverage on the catalyst sites, which can reduce the cell current density significantly. Otherwise, a significant rise in the θ_{CO} from 0.5 to 0.94 at the range from 10 to 100 ppm CO is found in Fig. 8.

Fig. 9 presents the total cell current density distributions across the anode catalyst layer under various ppm levels of CO. The predicted CO poisoning results are compared with the experimental data of Oetjen et al. [28]. A current density of nearly $1\,A\,cm^{-2}$ was obtained at $\eta_a = 0.01$ in the present results without CO contained. The experimental data were subjected to different CO concentration polarization curves at a 0.6 V cell voltage which corresponds to a CO-free at current density of

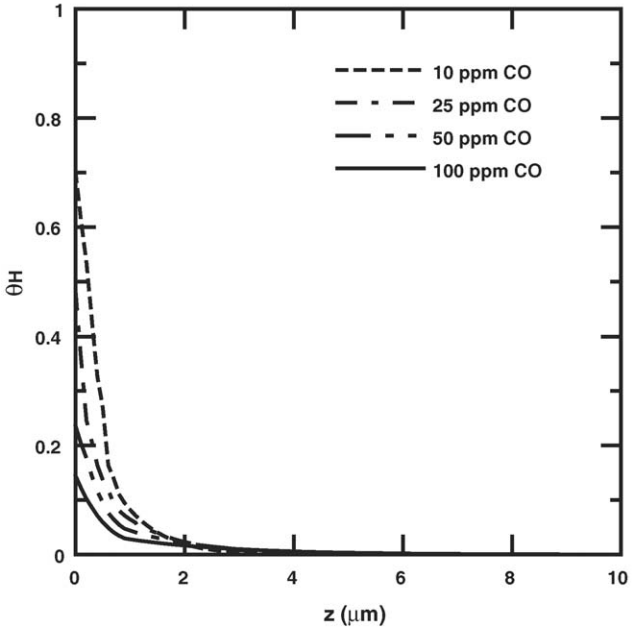

Fig. 7. Distributions of θ_H at steady state across the anode catalyst layer for different CO concentration with $\varepsilon_c = 0.4$, $\eta_a = 0.01$, and $L_c = 10\,\mu m$.

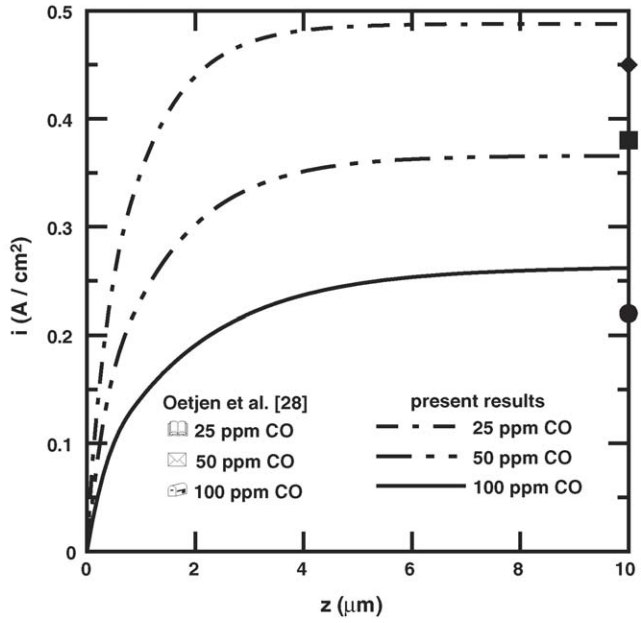

Fig. 9. Distributions of current density at steady state across the anode catalyst layer for different CO concentrations with $\varepsilon_c = 0.4$, $\eta_a = 0.01$, and $L_c = 10\,\mu m$.

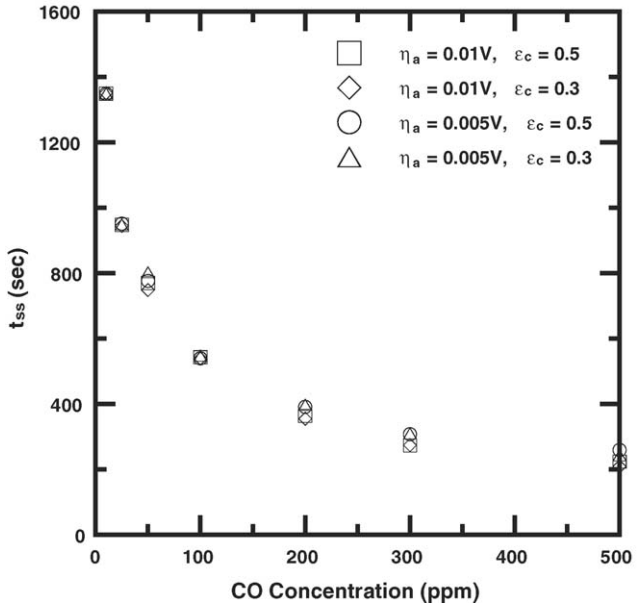

Fig. 10. Effects of the ppm CO concentration on the response time interval for different anode overpotentials η_a and gas porosities ε_c with $L_c = 10\,\mu m$.

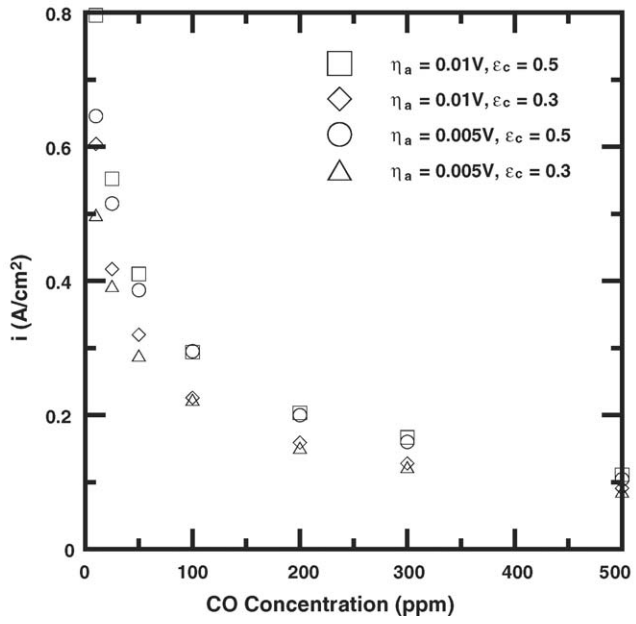

Fig. 11. Effects of the ppm CO concentration on the current density for different anode overpotentials η_a and gas porosities ε_c with $L_c = 10\,\mu m$.

1 A cm^{-2}. As shown in Fig. 9, the results show a good agreement with experimental data. A careful examination of Fig. 9 discloses that the current density would decrease from 1 to 0.487, 0.365 or 0.263 A cm^{-2} when the hydrogen is subjected to 25, 50 or 100 ppm CO, respectively. The predicted steady-state current density under different ppm levels of CO is consistent with Oetjen et al. [28].

As mentioned above, the hydrogen with various CO concentration not only drops the cell current density but also affects the response time interval t_{ss}. Fig. 10 shows the effects of the ppm levels of CO on the response time interval t_{ss} for different anode overpotentials and gas porosity. An overall inspection of Fig. 10 indicates that the ppm of CO has a significant impact on the response time interval. This is because the hydrogen with a high CO concentration would increase the CO adsorption on the catalyst sites, which in turn, causes a decrease in the response time interval t_{ss}. While the overpotential and gas porosity have a slight influence on the response time interval. The rate of hydrogen oxidation reactions increase exponentially with the anode overpotential which drastically consumed hydrogen fuel at the anode catalyst sites. This result decreases the hydrogen coverage. Although, the rate of CO oxidation reaction increases at the same time, it also raises the possibility of adsorbed CO on the catalyst sites. Therefore, the response time t_{ss} shows slight differences for different anode overpotentials. In addition, the response time interval decreases with an increase in CO.

Fig. 11 presents the variations of current density with CO concentration under different anode overpotential and gas porosity. It is seen that with a higher anode overpotential or gas porosity at the catalyst layer one can obtain a much greater current density, especially at low CO concentrations. This can be made plausible by noting the fact that the catalyst layer with a high porosity, the hydrogen fuel can be easily fed into the catalyst layer and a high anode overpotential can free up the catalyst reacting sites for hydrogen oxidation by bringing about the CO oxidation. With a 0.01 V anode overpotential and 10 ppm CO, the corresponding current density is 0.79 and 0.6 A cm^{-2} for porosity of 0.5 and 0.3, respectively. But, when the CO concentration is increased, the effects of the gas porosity on the current density would become less significant. A similar trend can be obtained for the case of an overpotential of 0.005 V at the same gas porosity under various CO concentrations.

3. Conclusions

The transient analysis of carbon monoxide poisoning at the anode catalyst layer is investigated. The CO kinetic model developed by Springer et al. [19] was adopted and extended to simulate thetransient characteristics of the CO poisoning process. In this theoretical model, the catalyst layer is treated as a thin film instead of an interface in order to investigate the response time interval required to reach the steady state under different conditions. Current density distribution, reactant gas distribution, and the coverage across the anode catalyst layer are also investigated. The relevant parameters include various levels of CO concentration, anode overvoltage, and gas porosity leading to the following conclusions:When carbon monoxide exists in the hydrogen fuel, the cell performance decreases with an increase in the CO concentration. As a result, the θ_H decreases with increasing CO concentration, which in turn, causes a low hydrogen electro-oxidation.The response time interval needed to reach the steady state condition, t_{ss}, is strongly influenced by the CO concentrations. This is due to the fact that the CO electro-oxidation is insufficient to free up the catalyst sites. Therefore, it is easy for CO to accumulate on the Pt catalyst site with high levels of CO concentration which decrease the hydrogen oxidation,

which in turn, causes a decrease in the response time interval, t_{ss}.A better cell performance can be obtained for a system with a higher overpotential or gas porosity, especially at low levels of CO. This is because for a case with high porosity, the hydrogen fuel can be easily fed into the catalyst layer and a high anode overpotential can free up the catalyst sites for hydrogen oxidation by bringing about greater CO oxidation.Effects of the CO levels have a significant impact on the response time interval, especially for low levels of CO.

Acknowledgement

The study was supported by the National Science Council, the Republic of China, through the grants NSC 93-2212-E-009-001.

References

[1] R.C. Urian, A.F. Gulla, S. Mukerjee, J. Electroanal. Chem. 554–555 (2003) 307–324.
[2] J. Zhang, R. Datta, J. Electrochem. Soc. 149 (2002) A1423–A1431.
[3] T. Okada, Y. Ayato, M. Yuasa, I. Sekine, J. Phys. Chem. B 103 (1999) 3315–3322.
[4] T. Okada, H. Satou, M. Okuno, M. Yuasa, J. Phys. Chem. B 106 (2002) 1267–1273.
[5] T. Okada, Y. Ayato, J. Dale, M. Yuasa, I. Sekine, O. Andreas, PCCP 2 (2002) 3255–3261.
[6] T. Okada, J. Electroanal. Chem. 465 (1999) 1–17.
[7] T. Okada, J. Electroanal. Chem. 465 (1999) 18–29.
[8] R. Halseid, J.S. Vie Preben, R. Tunold, J. Electrochem. Soc. 151 (2004) A381–A388.
[9] F.A. Uribe, S. Gottesfeld, T.A. Zawodzinski, J. Electrochem. Soc. 149 (2002) A293–A296.
[10] Y. Si, R. Jiang, J.C. Lin, H.R. Kunz, J.M. Fenton, J. Electrochem. Soc. 151 (2004) A1820–A1824.
[11] J. Zhang, T. Thampan, R. Datta, J. Electrochem. Soc. 149 (2002) A765–A772.
[12] H. Yu, Z. Hou, B. Yi, Z. Lin, J. Power Sources 105 (2002) 52–57.
[13] E.I. Santiago, V.A. Paganin, M. do Carmo, E.R. Gonzalez, E.A. Ticianelli, J. Electroanal. Chem. 575 (2005) 53–60.
[14] Z. Qi, C. He, A. Kaufman, J. Power Sources 111 (2002) 239–247.
[15] Z. Jusys, J. Kaiser, R.J. Behm, J. Electroanal. Chem. 554–555 (2003) 427–437.
[16] P.A. Adock, S.V. Pacheco, K.M. Norman, F.A. Uribe, J. Electrochem. Soc. 152 (2005) A459–A466.
[17] A.H. Thomason, T.R. Lalk, A.J. Appleby, J. Power Sources 135 (2004) 204–211.
[18] L.P.L. Carrete, K.A. Friedrich, M. Hubel, U. Stimming, Phys. Chem. 3 (2001) 320–324.
[19] T.E. Springer, T. Rockward, T.A. Zawodzinski, S. Gottesfeld, J. Electrochem. Soc. 148 (2001) A11–A23.
[20] S.H. Chan, S.K. Goh, S.P. Jiang, Electrochim. Acta 48 (2003) 1905–1919.
[21] D.M. Bernardi, M.W. Verbrugge, J. Electrochem. Soc. 37 (1991) 1151–1163.
[22] D.M. Bernardi, M.W. Verbrugge, J. Electrochem. Soc. 139 (1992) 2477–2490.
[23] K.K. Bhatia, C.Y. Wang, Electrochim. Acta 49 (2004) 2333–2341.
[24] J.J. Baschuk, X. Li, Int. J. Energy Res. 25 (2001) 695–713.
[25] J.J. Baschuk, X. Li, Int. J. Energy Res. 27 (2003) 1095–1116.
[26] J.J. Baschuk, A.M. Rowe, X. Li, ASME J. Energy Resour. Technol. 125 (2003) 94–100.
[27] J.J. Baschuk, X. Li, Int. J. Global Energy Iss. 20 (2003) 245–276.
[28] H.F. Oetjen, V.M. Schmit, U. Stimming, F. Trila, J. Electrochem. Soc. 143 (1996) 3838–3842.